Improved Wavefront Reconstruction and Correction Strategy for Adaptive Optics System With a Plenoptic Sensor

Jintian Hu, Tao Chen, Xudong Lin, Liang Wang, Qichang An, and Zhichong Wang

***Abstract*—Wavefront reconstruction and correction under strong turbulence has become a crucial issue for adaptive optics systems. An approach using a plenoptic sensor has attracted high attention recently. However, the existing reconstruction and correction algorithms based on the plenoptic sensor are sometimes unsatisfactory. Therefore, we propose a modified approach based on the checkerboard algorithm to reconstruct the wavefront. By means of a weighted summation, the reconstruction accuracy is clearly increased. We propose using the direct-gradient method to correct the disturbed wavefront after reconstruction, and our experimental results demonstrate the effectiveness with only one correction step.**

***Index Terms*—plenoptic sensor, wavefront reconstruction, wavefront correction.**

I. Introduction

ADAPTIVE optics technology has been widely used to correct the wavefront distortion caused by atmospheric turbulence [1]. A wavefront sensor is often employed for wavefront detection, and a deformable mirror is employed for the correction. The Shack–Hartmann(S–H) wavefront sensor, which is the most widely used wavefront sensor, has been proven effective under weak turbulence conditions. However, the S-H wavefront sensor will encounter challenges in strong turbulence scenarios [2]. It will have considerate trouble reconstructing wavefronts with problems such as scintillation and branch points caused by strong turbulence.

Manuscript received April 20, 2021; revised June 22, 2021; accepted July 13, 2021. Date of publication July 20, 2021; date of current version August 25, 2021. This work was supported in part by the Youth Innovation Promotion Association of the Chinese Academy of Sciences under Grant 2020221, in part by Natural Science Foundation of China under Grant 62005279, in part by Equipment Development Project of Chinese Academy of Sciences under Grant YJKYYQ20200057, and in part by the Innovation Program of Changchun Institute of Optics, Fine Mechanics and Physics, Chinese Academy of Sciences under Grant Y9S533B190. *(Corresponding author: Tao Chen; Liang Wang.)*

Jintian Hu and Zhichong Wang are with the Changchun Institute of Optics, Fine Mechanics and Physics, Chinese Academy of Sciences, Changchun 130025, China, and also with the University of Chinese Academy of Sciences, Beijing 100049, China (e-mail: 937472452@qq.com; 1250738690@qq.com).

Tao Chen, Xudong Lin, and Qichang An are with the Changchun Institute of Optics, Fine Mechanics and Physics, Chinese Academy of Sciences, Changchun 130033, China (e-mail: chent@ciomp.ac.cn; 13039222921@126.com; anjj@mail.ustc.edu.cn).

Liang Wang is with the Changchun Institute of Optics, Fine Mechanics and Physics, Chinese Academy of Sciences, Changchun 130033, China, and also with the School of Mechanical and Aerospace Engineering, Jilin University, Changchun 130025, China (e-mail: wangliang.ciomp@foxmail.com).

Digital Object Identifier 10.1109/JPHOT.2021.3098014

Various approaches have been proposed to overcome this problem. The use of a plenoptic camera for wavefront sensing is one option [3], [4]. With this solution, the wavefront can be estimated by measuring each individual micro-lens image. With the developments of the plenoptic sensing, a modified plenoptic sensor has been proposed by researchers at the University of Maryland College Park for wavefront detection [5]–[15]. It can simultaneously acquire the amplitude and phase information of the incident wavefront. Thereafter, the wavefront can be reconstructed under any turbulence conditions. The researchers have proposed two algorithms called checkerboard reconstruction algorithm and graph reconstruction algorithm to reconstruct and correct the wavefront [1]. However, the checkerboard algorithm does a good job, but it is time-consuming. The graph algorithm works quickly, but accuracy cannot be guaranteed. Therefore, there exists an untenable trade-off between speed and accuracy.

In this paper, we propose a modified checkerboard algorithm to determine the wavefront phase information. Subsequently, the direct-gradient method is used to correct the wavefront distortions. As a result, the wavefront can be reconstructed and corrected quickly with high accuracy.

The remainder of this article is organized as follows. The basic principles of the plenoptic sensor are introduced first in Section II. Then, we discuss the modified reconstruction algorithm, and present experimental results in Section III. In Section IV, the direct-gradient method is introduced to correct the wavefront. The study conclusions are summarized in Section V.

II. Principles of the Plenoptic Sensor

A. Basic Structure and Design

Several configurations of the plenoptic sensor have been developed for imaging purposes. Fig. 1 shows the basic structure of the plenoptic sensor we used. As can be seen, the plenoptic sensor contains an objective lens, a micro-lens array (MLA), and an image sensor. In Fig. 1, f_{obj} and d_{obj} represent the focal length and the diameter of the objective lens, respectively. The focal length and the pitch of the MLA are expressed as f_{MLA} and d_{MLA}, respectively. The back focal plane of the objective lens coincides with the front focal plane of the MLA. The image sensor is placed at the back focal plane of the MLA.

From Fourier optics, we can determine that the objective lens performs a 2-dimensional Fourier transform of the incident

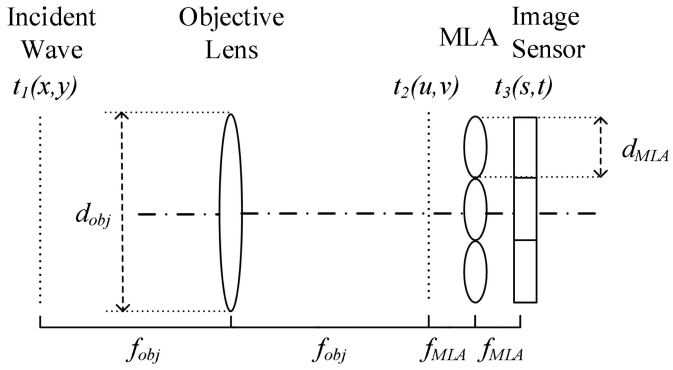

Fig. 1. Structure of the plenoptic sensor.

wavefront, $t_1(x,y)$, located at the front focal plane to the transformed wavefront, $t_2(u,v)$, located at the back focal plane [16]. Then the MLA performs another Fourier transform of $t_2(u,v)$ to the back focal plane of the MLA, $t_3(s,t)$. Finally we can acquire the plenoptic images on the image sensor. The two steps are expressed by (1) and (2) as follows:

$$t_2(u,v) = \frac{1}{j\lambda f_{obj}} \iint t_1(x,y) \exp\left\{\frac{-j2\pi}{\lambda f_{obj}}(ux+vy)\right\} dxdy \tag{1}$$

$$\begin{aligned} t_3(s,t) = \frac{1}{j\lambda f_{MLA}} \iint t_2(u,v) \sum_{M,N} \\ rect\left(\frac{u+s-2Md_{MLA}}{d_{MLA}}\right) rect\left(\frac{v+t-2Nd_{MLA}}{d_{MLA}}\right) \\ \exp\left\{\frac{-j2\pi}{\lambda f_{MLA}}(u-Md_{MLA})(s-Md_{MLA})\right. \\ \left. +(v-Nd_{MLA})(t-Nd_{MLA})\right\} dudv. \end{aligned} \tag{2}$$

In (2), *(M, N)* represents the coordinates of each MLA lens. To avoid overlapping of the MLA sub-images, the *f*-number of the objective lens should be no less than that of the MLA lenslet [9], [12], which can be expressed as:

$$\frac{d_{obj}}{f_{obj}} \leq \frac{d_{MLA}}{f_{MLA}}. \tag{3}$$

As Fig. 2 shows, if the incident beam is plane, the whole beam will only be imaged by the central MLA sub-aperture. The features of the incident beam will change if it is disturbed. It will be separated into different MLA sub-apertures according to the angular spectra of the wavefront [12]. Furthermore, the incident beam will be separated into more MLA sub-apertures when the turbulence gets stronger.

B. Performance Analysis

To make full use of a wavefront sensor, performance characteristics such as sensitivity and dynamic range must be considered. As is discussed in Ref [12], the sensitivity and dynamic range of the plenoptic sensor can be calculated by (4) and (5):

$$(\Delta x_{\min}, \Delta y_{\min}) = \frac{d_{MLA}}{f_{obj}} \tag{4}$$

$$\begin{aligned} (\Delta x_{\max}, \Delta y_{\max}) &= \frac{Sensor\_Width}{2 \times d_{MLA}} \times \frac{d_{MLA}}{f_{obj}} \\ &= \frac{Sensor\_Width}{2 \times f_{obj}} \end{aligned} \tag{5}$$

Equation (4) represents the calculation of the plenoptic sensor's sensitivity, which designates the minimum quantized wavefront tilt that can be measured by the plenoptic sensor. Eq. (5) represents the dynamic range of the plenoptic sensor, where *Sensor_Width* represents the width of the image sensor. By multiplying the sensitivity by the half number of the MLA sub-apertures that the image sensor owns in one direction, the maximum measurable tilt can be calculated.

It can be easily found that a small MLA pitch can improve the sensitivity of the plenoptic sensor. But we cannot reduce the pitch up to a point, where diffraction of the small lens may cause the loss of local features, such that reconstruction cannot be performed. Furthermore, a long focal length of the objective length can also improve the sensitivity, but the dynamic range will be reduced. As a result, a trade-off between the sensitivity and dynamic range should be made to obtain a high wavefront sensing ability.

III. Wavefront Reconstruction

A. Checkerboard Reconstruction Algorithm

According to the previous theoretical analyses, each MLA sub-aperture represents a specific angular spectrum area of the wavefront. Based on this knowledge, researchers at the University of Maryland College Park proposed a checkerboard reconstruction algorithm [1] that divided each MLA cell into smaller "checkerboard" units. They further divided those units in each MLA sub-aperture to represent different spatial positions of the incident wavefront.

Taking Fig. 3 as an example, we can start with a simple 3×3 MLA cell. Each MLA cell is then divided into four checkerboard units as "A", "B", "C", and "D" for simplicity. Each unit "A" in different sub-apertures represents the same spatial position of the incident wavefront regardless of the different angular spectra represented. Fig. 3 also shows the layout of a plane beam. The incident beam is only imaged by the center MLA cell as discussed before.

Fig. 4 describes the process of the checkerboard algorithm. When the incident beam is distorted, the entire beam will be separated into various MLA cells, just as shown in the left image of Fig. 4. In order to reconstruct the wavefront, we will examine each checkerboard unit to determine the local gradient at the corresponding location. Taking unit "A" as an example, we search for each MLA sub-aperture first and select the MLA sub-aperture having the largest pixel sum value in unit "A" area, which is cell $(-1,0)$ in Fig. 4, to represent the spatial wavefront information at the corresponding position. The same operation is performed for the remaining units. A map of the local gradients

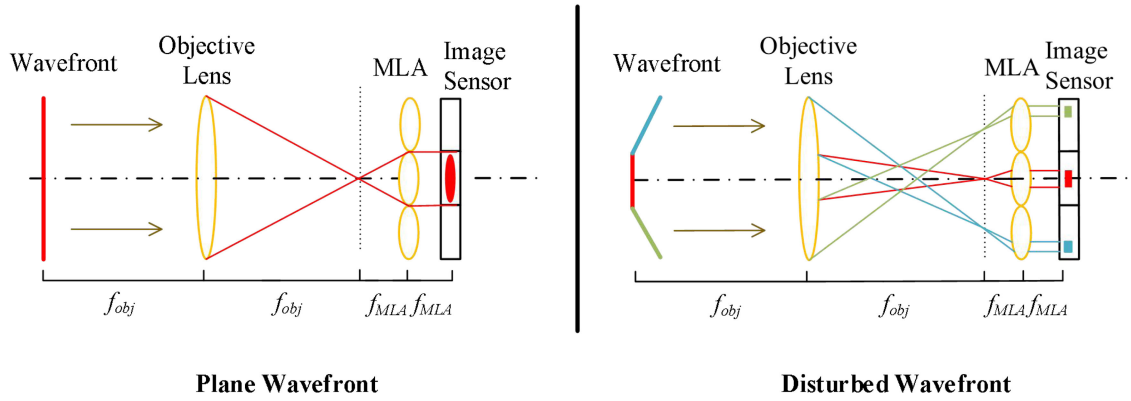

Fig. 2. Imaging diagram of the plenoptic sensor.

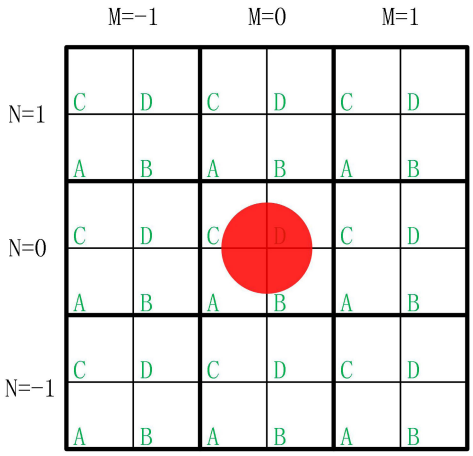

Fig. 3. Diagram of the checkerboard division and layout of plane beam.

for each checkerboard unit can then be acquired. By using the Zernike modal method, we can finally obtain the reconstructed wavefront.

B. Modified Checkerboard Reconstruction Algorithm

Sometimes the pixel-sum values for the same unit of the two or more MLA sub-apertures are extremely similar. In Fig. 5, unit "C" has a non-zero pixel value in three sub-apertures, which is cell(-1,1), cell(1,0) and cell(0,-1). The pixel-sum values are 180, 55 and 186, respectively. In this case, it would be inaccurate to select the largest intensity to represent the wavefront information. Therefore, we propose a modified approach.

After searching for all MLA sub-apertures, we select the largest two cells for each unit and perform a weighted summation, which can be expressed as:

$$M = \frac{V_1}{V_1 + V_2} M_1 + \frac{V_2}{V_1 + V_2} M_2 \tag{6}$$

$$N = \frac{V_1}{V_1 + V_2} N_1 + \frac{V_2}{V_1 + V_2} N_2. \tag{7}$$

In (6) and (7), (M_1, N_1) and (M_2, N_2) represent the coordinates of the MLA cells we selected, and V_1 and V_2 are their pixel sum values respectively. Instead of simply using the cell with the largest intensity, we choose the weighted value to represent the wavefront gradient information.

If the values of V_1 and V_2 are differed by a large amount, the coordinates (M, N) calculated by (6) and (7) will be extremely close to the sub-aperture coordinates having the largest intensity. Therefore, the wavefront gradient information will also be very similar. If the values of V_1 and V_2 are close, a large number of errors will be produced using the original checkerboard algorithm, the calculated wavefront gradient information will be more accurate after the weighted summation. Based on the above analysis, our approach effectively improves the accuracy of the reconstruction without increasing too much running time, which may be less than 0.1 seconds in our experiment.

Subsequently, the same operation as we discussed before is performed again here to reconstruct the wavefront. The overall procedure of our approach, which can be called the "top-2" method, is shown in the following algorithm:

Algorithm: Top-2 Reconstruction Algorithm.

Input: a plenoptic image, $Im(x, y)$
Output: the reconstructed wavefront image, *Wavefront_im*(x,y)

1: Separate each MLA sub-aperture into various checkerboard units.
2: **for** every checkerboard unit
3: Search for all the MLA sub-apertures, record the coordinates of (M_1, N_1) and (M_2, N_2), as well as their pixel sum values V_1 and V_2.
4: Obtain the target coordinates of (M, N) by using Eqs (6) and (7).
5: **end for**
6: Calculate the wavefront gradients for each checkerboard units through (M, N).
7: Reconstruct the wavefront with the use of gradients information by the Zernike modal method

C. Experimental Layout

To demonstrate that our approach is effective, we built an experimental platform based on the plenoptic sensor. The schematic and actual experimental layout are shown in Figs 6

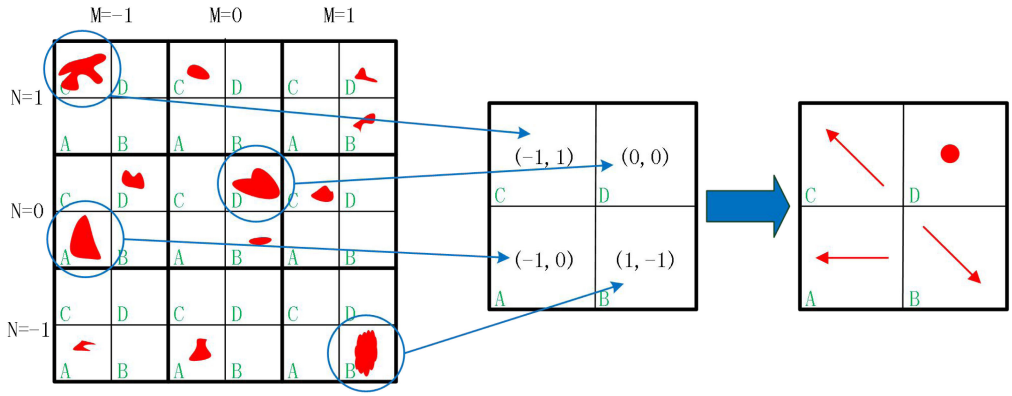

Fig. 4. Diagram of the checkerboard reconstruction.

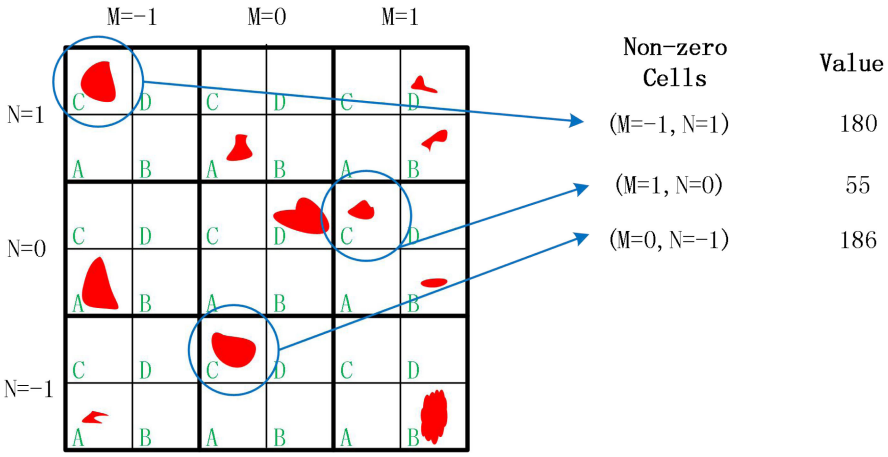

Fig. 5. Layout of special condition.

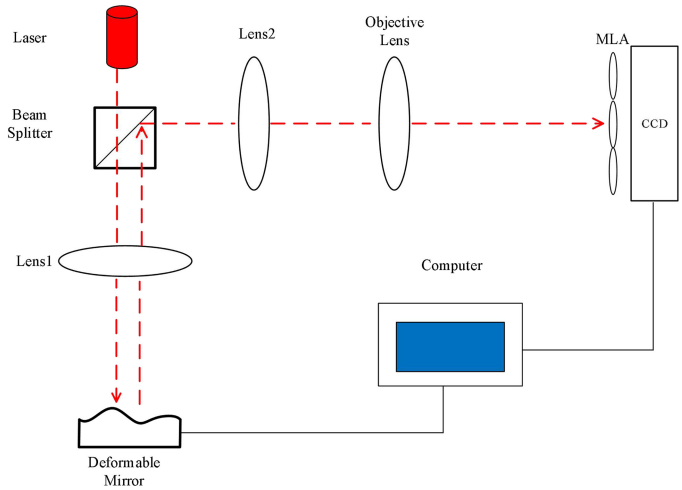

Fig. 6. Diagram of the experimental platform setup.

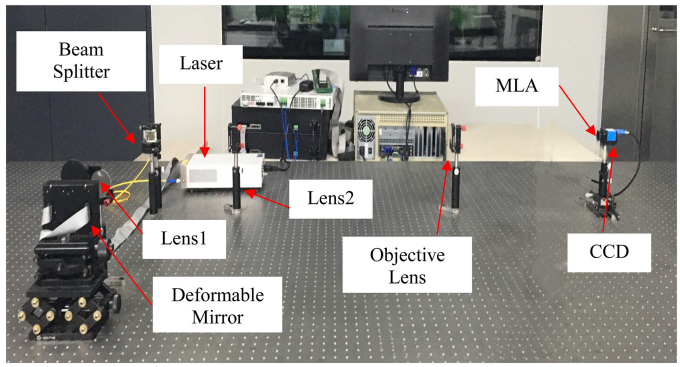

Fig. 7. Actual experimental layout.

and 7, respectively. A 633nm HeNe laser passes through a beam splitter into Lens1, creating a parallel beam that spreads to our 21-element deformable mirror. By controlling the deformable mirror, the reflected beam with distortion returns and then passes through the Lens1 and Lens2 shrink-beam group to avoid overlapping. Finally, the beam is spread to the plenoptic sensor.

Because the focal length and the pitch of our MLA are 7mm and 0.2mm, respectively, and the focal length of our objective lens is 500mm, the width of the incident beam should be no greater than 14mm. Fig. 8 shows the layout diagram of our deformable mirror. As it shows, the distance between neighbouring actuator is 7mm, and the diameter of our deformable mirror is 35mm, hence we use a shrink-beam group comprised by Lens1 having a focal length of 500mm and Lens2 having a focal length of 200mm to satisfy the restriction. The camera we used is DMK

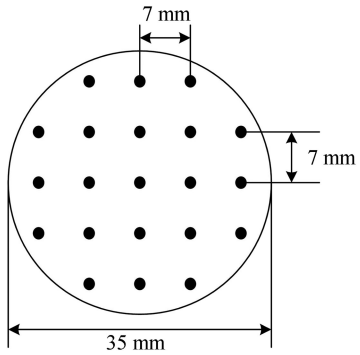

Fig. 8. Layout diagram of our 21-element deformable mirror actuators.

TABLE I
RECONSTRUCTED RESULTS OF 0.5λ DEFORMATION

	Aberration	Defocus	Astigmatism	Coma	Trefoil
Our approach	Zernike coefficient	0.518λ	0.469λ	0.511λ	0.520λ
	RMS	0.137λ	0.157λ	0.189λ	0.162λ
Original algorithm	Zernike coefficient	0.608λ	0.456λ	0.619λ	0.551λ
	RMS	0.235λ	0.160λ	0.265λ	0.199λ

TABLE II
RECONSTRUCTED RESULTS OF 1λ DEFORMATION

	Aberration	Defocus	Astigmatism	Coma	Trefoil
Our approach	Zernike coefficient	1.174λ	0.964λ	0.996λ	0.988λ
	RMS	0.274λ	0.163λ	0.138λ	0.149λ
Original algorithm	Zernike coefficient	0.958λ	1.036λ	1.065λ	0.911λ
	RMS	0.245λ	0.164λ	0.253λ	0.208λ

TABLE III
RECONSTRUCTED RESULTS OF 1.5λ DEFORMATION

	Aberration	Defocus	Astigmatism	Coma	Trefoil
Our approach	Zernike coefficient	1.637λ	1.439λ	1.456λ	1.499λ
	RMS	0.251λ	0.140λ	0.130λ	0.102λ
Original algorithm	Zernike coefficient	1.746λ	1.752λ	1.332λ	1.365λ
	RMS	0.321λ	0.323λ	0.337λ	0.273λ

23UM021 from the Imaging Source, which contains a 480×480 resolution with 7.5μm pixel width in the binning mode.

D. Results and Analysis

Various Zernike polynomials can be applied to the deformable mirror to create different Zernike deformations [17]. The polynomials we used are described as follows:

$$Defocus: Z_2^0(r,\theta) = \sqrt{3}(2r^2-1) \tag{8}$$

$$Astigmatism: Z_2^2(r,\theta) = \sqrt{6}r^2\sin(2\theta) \tag{9}$$

$$Coma: Z_3^1(r,\theta) = \sqrt{8}(3r^3-2r)\sin\theta \tag{10}$$

$$Trefoil: Z_3^3(r,\theta) = \sqrt{8}r^3\sin(3\theta). \tag{11}$$

In (8)–(11), (r,θ) represent the normalized radius and angle, respectively. Fig. 9 shows the images of the different Zernike deformations, but only a smaller 250×250 pixel section is displayed.

TABLE IV
RECONSTRUCTED RESULTS OF 2λ DEFORMATION

	Aberration	Defocus	Astigmatism	Coma	Trefoil
Our approach	Zernike coefficient	2.292λ	1.999λ	1.877λ	1.913λ
	RMS	0.307λ	0.207λ	0.248λ	0.185λ
Original algorithm	Zernike coefficient	2.345λ	2.445λ	1.701λ	1.773λ
	RMS	0.408λ	0.454λ	0.405λ	0.383λ

TABLE V
RESULTS OF 0.5λ DEFORMATION AFTER CORRECTION

	Aberration	Defocus	Astigmatism	Coma	Trefoil
RMS	Our approach	0.078λ	0.097λ	0.091λ	0.089λ
	Original algorithm	0.116λ	0.107λ	0.209λ	0.118λ

TABLE VI
RESULTS OF 1λ DEFORMATION AFTER CORRECTION

	Aberration	Defocus	Astigmatism	Coma	Trefoil
RMS	Our approach	0.096λ	0.100λ	0.121λ	0.156λ
	Original algorithm	0.246λ	0.175λ	0.212λ	0.165λ

To demonstrate the effectiveness of our approach, both algorithms were used to reconstruct the wavefront of the images obtained previously. In our experiment, the total plenoptic image is 480×480 pixel, and the MLA we used is 15×15. We divide each MLA sub-aperture into 64 checkerboard units, and the size of each checkerboard unit is 3×3 pixel.

Fig. 10 shows the reconstructed results of Astigmatism for two algorithms. A two-wavelength deformation was applied to the deformable mirror. Fig. 9(c) shows the image obtained from the plenoptic sensor. Fig. 10(a) is the result of the reconstructed wavefront using the original checkerboard reconstruction algorithm. Fig. 10(c) separates the reconstructed result into different Zernike modes. Figs 10(b) and (d) represent the same results after improvement.

It is obvious from Figs 10(a) and (b) that the reconstructed wavefront is the result of Astigmatism. In Figs 10(c) and (d), we can see that Zernike mode 5, which represents the Zernike deformation of Astigmatism, is the dominant mode. This also demonstrates the effectiveness of both reconstruction algorithms. Moreover, the value of the Zernike coefficient is 2.445λ and the root-mean-square (RMS) phase reconstruction error is 0.454λ using original checkerboard algorithm. The RMS phase reconstruction error is calculated by:

$$RMS = \sqrt{\sum_{i=1}^{10}\left(Z_{rec}(i) - Z_{input}(i)\right)^2} \tag{12}$$

where Z_{input} represents the input coefficients of the various Zernike modes, Z_{rec} represents the reconstructed coefficients of the various Zernike modes, and *i* represents the index of the

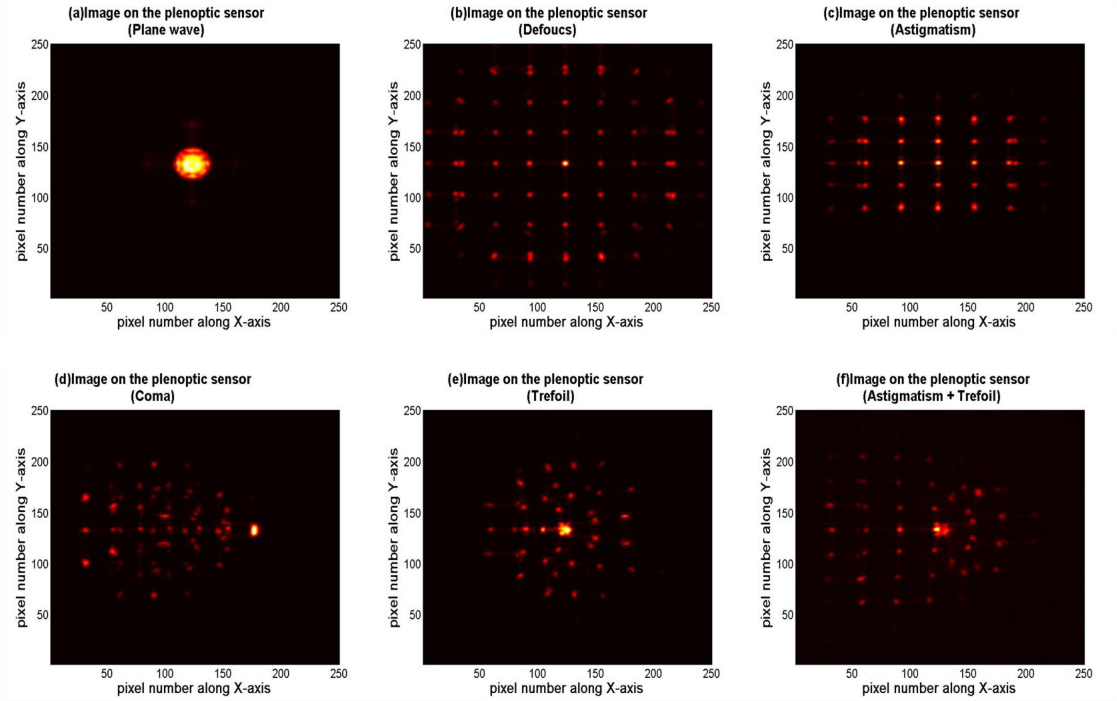

Fig. 9. Plenoptic images of different Zernike deformations.

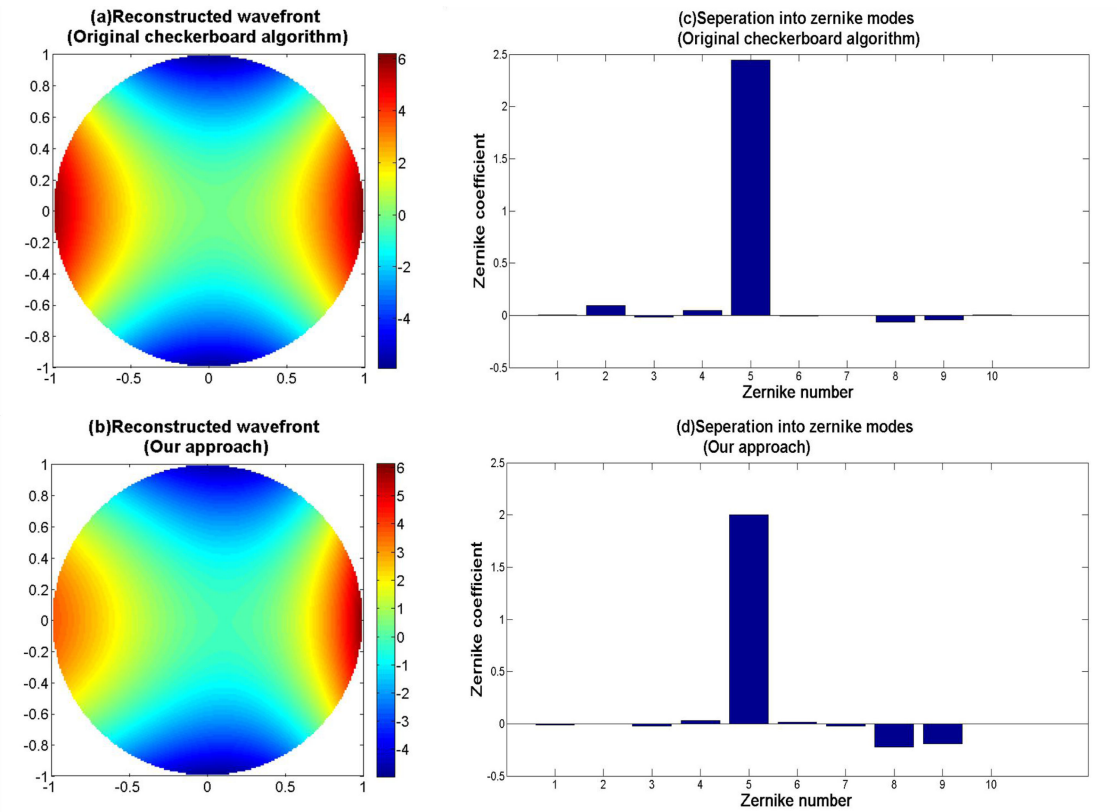

Fig. 10. Reconstruction of Astigmatism.

TABLE VII
RESULTS OF 1.5λ DEFORMATION AFTER CORRECTION

	Aberration	Defocus	Astigmatism	Coma	Trefoil
RMS	Our approach	0.101λ	0.153λ	0.154λ	0.102λ
	Original algorithm	0.264λ	0.295λ	0.338λ	0.329λ

TABLE VIII
RESULTS OF 2λ DEFORMATION AFTER CORRECTION

	Aberration	Defocus	Astigmatism	Coma	Trefoil
RMS	Our approach	0.076λ	0.145λ	0.150λ	0.183λ
	Original algorithm	0.301λ	0.342λ	0.371λ	0.374λ

Zernike coefficients. The results respectively drop to 1.999λ and 0.207λ after improvement, which demonstrates that a higher reconstruction accuracy is obtained with our approach.

More reconstructed results can be found in Tables I–IV. It can be concluded that our approach results in a lower error for most of the cases and comparable results for the corner cases.

IV. WAVEFRONT CORRECTION

A. Direct-Gradient Method

Because the reconstructed wavefront gradient reflects the wavefront distortion information, through correction of the wavefront gradient error, the overall distortion can be effectively corrected. Therefore, after the wavefront gradient is determined, the direct-gradient method can be used to correct the distortion [18]–[21]. Generally, there is a linear relationship between the local gradient and the drive voltages of the deformable mirror actuators, which can be expressed as:

$$G = D \cdot V \tag{13}$$

where $G = [g_{1x}, g_{1y}, \ldots g_{mx}, g_{my}]^T$ is the vector of the wavefront gradients, and m is the number of the checkerboard units, which is 64 in our experiment. $V = [v_1, v_2, \ldots v_n]^T$ is the vector of the drive voltages, and n is the number of the actuators employed for our deformable mirror, which is 21 in our experiment. D is a $2m \times n$ constant matrix called the influence matrix, which bridges the deformable mirror to our plenoptic sensor.

By recording the gradients response and the driving voltages for the various determined deformations, the influence matrix D can be easily acquired. After the influence matrix D is determined, we can easily obtain the correction voltage for any incoming wave by:

$$V = D^+ \cdot G \tag{14}$$

where D^+ is the pseudo inverse of matrix D.

B. Results and Analysis

To demonstrate that the above discussions are effective, we allow the direct-gradient method to correct the disturbed plenoptic images we get before. Some experimental results using our modified algorithm are shown in Fig. 11. Fig. 11(b) shows the result of Astigmatism after one correction step. We can see that the entire beam almost locates in single MLA cell and the RMS error drops to 0.100λ, which means a nearly plane wavefront. Compared with the work in Ref [1], it costs 5 correction steps to remove the major distortion. More correction results can be found in Tables V–VIII, which demonstrates the quickness and the effectiveness of our method.

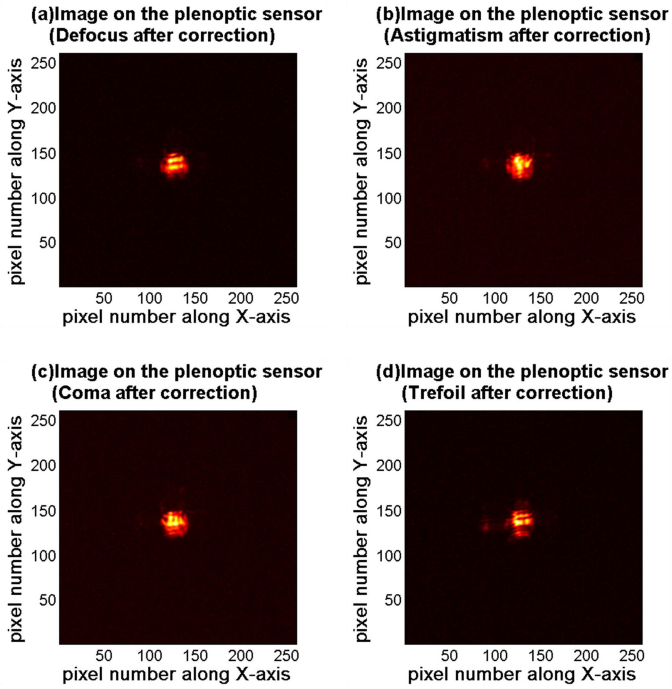

Fig. 11. Correction of different Zernike deformations.

To further prove the effectiveness of our modified algorithm, original checkerboard algorithm is also used for correction. Tables V–VIII also present the detailed results after one correction step using the original algorithm. It can be seen that with a higher reconstruction accuracy obtained by our approach, a better correction result can also be acquired.

V. CONCLUSION

In this paper, we propose a modified checkerboard reconstruction algorithm based on the plenoptic sensor. A weighted summation is added to acquire the wavefront gradient information. Subsequently, we build an experimental platform to validate the effectiveness of our approach. The experimental results demonstrate that a higher reconstruction accuracy can be obtained after improvement. Moreover, we propose to use the direct-gradient method to correct the wavefront distortion. After determination of the influence matrix and the wavefront gradients by calculation, distortions can then be corrected quickly and effectively. The experimental results indicate that most distortions can be removed after only one step of correction.

ACKNOWLEDGMENT

The authors would like to thank anonymous reviewers for their helpful suggestions and Editage (www.editage.cn) for English language editing.

REFERENCES

[1] J. Ko, C. Wu, and C. C. Davis, "An adaptive optics approach for laser beam correction in turbulence utilizing a modified plenoptic camera," *Laser Commun. Propag. Through Atmos. Oceans IV*, vol. 9614, 2015, Art. no. 96140I.

[2] A. T. Watnik and D. F. Gardner, "Wavefront sensing in deep turbulence," *Opt. Photon. News*, vol. 29, no. 10, pp. 38–45, 2018.

[3] P. Jiang, J. Xu, Y. Liang, and H. Mao, "Comparision of the shack-hartmann and plenoptic sensor in closed-loop adaptive optics system," *Opt. Eng.*, vol. 55, no. 3, 2016, Art. no. 033105.

[4] J. Rodríguez-Ramos, B. Femenía Castellá, F. P. Nava, and S. Fumero, "Wavefront and distance measurement using the CAFADIS camera," *Adaptive Opt. Syst.*, vol. 7015, 2008, Art. no. 70155Q.

[5] C. Wu and C. C. Davis, "Modified plenoptic camera for phase and amplitude wavefront sensing," *Laser Commun. Propag. through Atmos. Oceans II*, vol. 8874, 2013, Art. no. 88740I.

[6] C. Wu, J. Ko, W. Nelson, and C. C. Davis, "Phase and amplitude wave front sensing and reconstruction with a modified plenoptic camera," *Laser Commun. Propag. through Atmos. Oceans III*, vol. 9924, 2014, Art. no. 92240G.

[7] C. Wu, J. Ko, and C. C. Davis, "Determining the phase and amplitude distortion of a wavefront using a plenoptic sensor," *J. Opt. Soc. Amer.*, vol. A32, no. 5, pp. 964–978, 2015.

[8] C. Wu, J. Ko, and C. C. Davis, "Complex wavefront sensing with a plenoptic sensor," *Laser Commun. Propag. through Atmos. Oceans V*, vol. 9979, 2016, Art. no. 99790Y.

[9] C. Wu, J. Ko, and C. C. Davis, "Plenoptic mapping for imaging and retrieval of the complex field amplitude of a laser beam," *Opt. Exp.*, vol.vol. 24, no. 26, pp. 29852–29871, 2016.

[10] C. Wu, J. Ko, and C. C. Davis, "Imaging through strong turbulence with a light field approach," *Opt. Exp.*, vol. 24, no. 11, pp. 11975–11986, 2016.

[11] C. Wu, J. Ko, and C. C. Davis, "Using a plenoptic sensor to reconstruct vortex phase structures," *Opt. Lett.*, vol. 41, no. 14, pp. 3169–3172, 2016.

[12] J. Ko and C. C. Davis, "Comparison of the plenoptic sensor and the Shack- Hartmann Sensor," *Appl. Opt.*, vol. 56, no. 13, pp. 3689–3698, 2017.

[13] C. Wu, D. A. Paulson, J. R. Rzasa, and C. C. Davis, "Comparison between the plenoptic sensor and the light field camera in restoring images through turbulence," *OSA Continuum*, vol. 2, no. 9, pp. 2511–2525, 1019.

[14] C. Wu, D. A. Paulson, J. R. Rzasa, and C. C. Davis, "Extracting phase distortion from laser glints on a remote target using phase space plenoptic mapping," *J. Opt. Soc. Amer. B*, vol. 36, no. 7, pp. 1964–1971, 2019.

[15] C. Wu, J. Ko, and C. C. Davis, "Lossy wavefront sensing and correction of distorted laser beams," *Appl. Opt.*, vol. 59, no. 3, 2020, Art. no. 817.

[16] J. Goodman, "Wave-optics analysis of coherent optical systems," in *Introduction to Fourier Optics*, 2nd ed. L. Cox and J. M. Morriss, Eds. New York, NY, USA: McGraw-Hill, 1996, pp. 101–107.

[17] R. Tyson, *Principles of Adaptive Optics*, 3rd ed., Boca Raton, FL, USA: CRC Press, 2011, pp. 187–189.

[18] E. P. Wallner, "Optimal wavefront correction using slope measurements," *JOSA*, vol. 73, no. 12, pp. 1171–1176, 1983.

[19] X. Li, C. Wang, H. Xian, and W. Jiang, "Control effect analysis for a Direct-gradient wave-front reconstruction algorithm," *Opto-Elect. Eng.*, vol. 25, no. 6, pp. 9–14, 1998.

[20] X. Li, C. Wang, H. Xian, and W. Jiang, "Zernike modal compensation analysis for an adaptive optics system using direct-gradient wave-front reconstruction algorithm," *Adaptive Opt. Syst. Technol.*, vol. 3762, pp. 116–124, 1999.

[21] X. Li and W. Jiang, "Comparing zonal reconstruction algorithms and modal reconstruction algorithms in adaptive optics system," *High-Resolution Wavefront Control: Methods, Devices, Appl. IV*, vol. 4825, pp. 121–130, 2002.